metals

MDPI

Article

Fe-X-B-Cu (X = Nb, NiZr) Alloys Produced by Mechanical Alloying: Influence of Milling Device

Albert Carrillo, Joan Saurina, Lluisa Escoda and Joan-Josep Suñol *

Department of Physics, University of Girona, C/Universitat de Girona 3, 17003 Girona, Spain; albert.carrillo.berlanga@gmail.com (A.C.); joan.saurina@udg.edu (J.S.); lluisa.escoda@udg.edu (L.E.)
* Correspondence: joanjosep.sunyol@udg.edu; Tel.: +34-872418757

Abstract: In this work, we analyze the influence of the milling device in the microstructural evolution of two Fe-X-B-Cu (X = Nb, NiZr) alloys produced by mechanical alloying (MA). The two milling devices are a planetary mil (P7) and a shaker mill (SPEX 8000). Microstructural analysis by X-ray diffraction detects the formation of a Fe rich solid solution. In the Fe-Nb-B-Cu alloy produced in the shaker mill also appears a Nb(B) minor phase, whereas in the Fe-NiZr-B-Cu alloy produced in the planetary mill, a minor disordered phase is formed. The comparative study regarding the energy transferred per unit of time in both devices determines that the shaker mill is more energetic. This fact explains that in the Fe-Nb-B-Cu alloy, Nb has not been introduced in the main Fe rich phase, whereas in the Fe-NiZr-B-Cu alloy milled in the shaker mill was formed the highly disordered phase. With regard to thermal analysis, the values of the apparent activation energies of the main crystallization process (above 200 kJ/mol) correspond to the crystalline growth of the nanocrystalline Fe rich phase.

Keywords: mechanical alloying; microstructure; Fe based alloys

Citation: Carrillo, A.; Saurina, J.; Escoda, L.; Suñol, J.-J. Fe-X-B-Cu (X = Nb, NiZr) Alloys Produced by Mechanical Alloying: Influence of Milling Device. *Metals* **2021**, *11*, 379. https://doi.org/10.3390/met11030379

Academic Editor: Tomasz Czujko

Received: 21 January 2021
Accepted: 21 February 2021
Published: 25 February 2021

1. Introduction

Nanocrystalline soft magnetic alloys have been obtained by rapid solidification techniques as melt-spinning, MS, (ribbon shape) or by mechanical alloying, MA (powder shape) [1,2]. Melt-spun ribbons are usually amorphous and further annealing is needed to develop nanocrystalline structure by primary crystallization [3]. Mechanical alloying favors the direct formation of powdered nanocrystalline alloys, that can be compacted/sintered to produce bulk pieces [4].

The nanocrystalline alloys can be classified based on the crystallographic structure of the nanocrystalline phase. The bcc Fe based alloys developed by Suzuki and coworkers are known as Nanoperm [5]. Nanoperm alloys, particularly nanocrystalline Fe-(Zr, Nb)-B-Cu alloys, have good magnetic properties: High effective permeability (~20,000) and low coercivity (<3 A/m) and core loss (<100 W/kg) at room temperature. There are soft magnetic offering reduced core losses over a wide range of applied frequencies. These alloys are an alternative for industrial (automotive, green energy) applications: High precision energy meters, absorber cores for suppression of motor bearing currents, high frequency current transformers, push-pull transformers for power transistors, and current sensors [3,4,6]. Due to magnetocaloric effect of the ferromagnetic to paramagnetic transition, these materials have also been of interest for magnetic refrigeration [7]. The composition is a key factor. It is known that an excessive content of B favors the formation of an amorphous phase, as it was found in $Fe_{75}Nb_{10}B_{15}$ [8], the increase of the coercivity and a decrease of the magnetization of saturation [9].

In the mechanical alloying process, the processing parameters influence the final microstructure and the functional properties. Milling parameters include the milling intensity, time and atmosphere, the ball-to-power weight ratio (BPR), the addition of a process control agent (PCA), and the filling factor of the vials. Some parameters, such as

PCA, are linked to grain refinement [10], but the majority has a high influence in the energy transferred to the powders [11].

In this work, two Nanoperm alloys ($Fe_{80}Nb_7B_{12}Cu_1$ and $Fe_{80}(NiZr)_7B_{12}Cu_1$) have been produced in two milling devices (shaker mill, planetary ball mill) to detect their influence on the nanocrystalline bcc Fe rich phase formation. In the SPEX 8000 shaker mill, the jar containing powders is agitated at a high frequency in a complex cycle that involves motion in three orthogonal directions (combining back-and-forth swings with short lateral movements, each end of the vial describing a figure like an eight). In the P7 planetary mill, two jars are arranged eccentrically on a platform (opposite direction of rotation between platform and jars). Furthermore, crystallographic microstructure (after 80 h MA) was discussed by energy transfer models.

2. Materials and Methods

Mechanical alloying has been performed in a Spex 800 shaker mill (Spex, Metuchen, NJ, USA) and in a Fritsch Pulverisette 7 planetary mill (Fritsch, Idar-Oberstein, Germany). The experiments were performed in jars sealed inside an Ar-filled glove box to prevent oxidation. The milling (10 g of powders) was performed in both devices with Cr-Ni steel jars (45 mL capacity) and balls (7 balls, 12 mm diameter) for 5, 20, and 80 h. The initial filling factor was close to one half. In SPEX, the information by the provider is that the number of cycles (rotational speed or frequency of rotation) is 875 rpm, whereas in the P7, the selected cycles of the platform, Ω, and jars, ω, are the same, 600 rpm. The R radius of the platform (measured from the geometric center of the jar position to the center of the platform) of the P7 is r_p = 7 cm and the internal radius of the jars r_j = 1.7 cm. The internal radius of the SPEX jar is 2.1 cm. The ball radius r_b is 0.6 cm in the Spex and 0.5 in the P7. The ball to powder weight ratio, BPR, used in both devices has been the same: 5.

The nominal composition of the two produced alloys were $Fe_{80}Nb_7B_{12}Cu_1$ and $Fe_{80}(NiZr)_7B_{12}Cu_1$ (at.%), labelled as A and B, respectively. Thus, depending on the mill device, the samples are labelled as: P7—A, SPEX—A, P7—B and SPEX—B. Elemental Fe, Nb, B, Cu powders, and NiZr compound (Sigma-Aldrich, Saint Louis, MO, USA) with high purity (<99.5%) and low particle size (Fe and Cu ~ 10 μm, B, B and Nb ~ 10 μm, NiZr < 100 μm) are mixed to obtain the desired composition. Likewise, NiZr compound was selected to avoid undesired oxidation of Zr.

The morphology, microstructure, and thermal behavior evolution as a function of milling time has been analyzed by scanning electron microscopy (SEM) coupled with compositional EDS spectroscopy microanalysis, X-Ray diffraction (XRD), and differential scanning calorimetry (DSC). SEM observations and EDS microanalysis were performed in a D500 device (Siemens/Bruker, Billerica, MA, USA); at least five micrographs/microanalyses for samples milled for 80 h. Thermal analysis was performed in a DSC822e calorimeter (Mettler-Toledo, Columbus, OH, USA); one experiment at 20 K/min for samples milled for 5 and 20 h, and four experiments for samples milled for 80 h. XRD experiments (before milling and after 5, 20, and 80 h of milling) were performed in a D8 Advance diffractometer (Siemens/Bruker, Billerica, MA, USA) using Cu-Kα radiation. XRD patterns analysis was performed by applying Rietveld refinement and the free software MAUD (Maud, Trento, Italy) [12].

3. Results and Discussion

3.1. Microstructure and Thermal Analysis

The XRD diffraction patterns of alloys A and B are given in Figures 1 and 2, respectively. The main component is elemental Fe in both alloys. Thus, as expected, the main phase (higher reflections intensity) in all the diffraction patterns is the bcc Fe phase. The reflection peaks of this phase are (110), (200), (211), and (220). The minor peaks before milling correspond to Cu, Nb, and NiZr compound. Initial elemental B was amorphous. These reflections disappear after milling. The minor elements were introduced in solid solution in the bcc Fe rich phase, or remains in the grain boundaries [8,9]. Regarding the shape of the

peaks, its width has increased considerably with the milling time, phenomena associated to a decrease in the crystalline size. The parameter of the goodness of fit, GOF, obtained from Rietveld refinement is lower than 1.25 for all XRD patterns. Regarding the shape of the peaks, its width has increased considerably with the milling time that seems to indicate a decrease in the crystalline size.

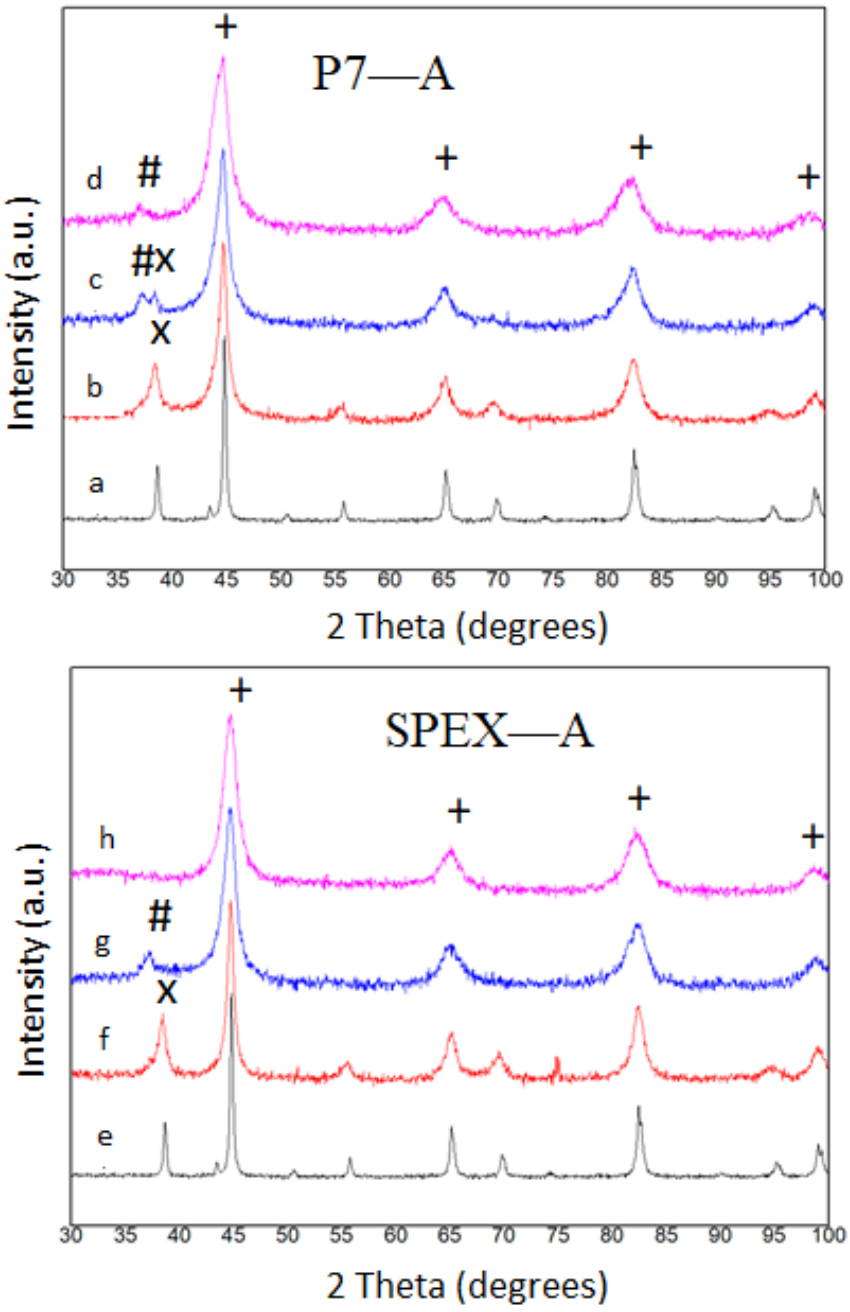

Figure 1. XRD (X-Ray diffraction) patterns of alloy A ($Fe_{80}Nb_7B_{12}Cu_1$). In the P7: (**a**) Before milling (0 h) and after milling ((**b**) 5 h, (**c**) 20 h, (**d**) 80 h); or in the Spex mill: (**e**) Before milling (0 h) and after milling ((**f**) 5 h, (**g**) 20 h, (**h**) 80 h). Bcc Fe rich solid solution (+), Nb phase (X), Nb(B) phase (#).

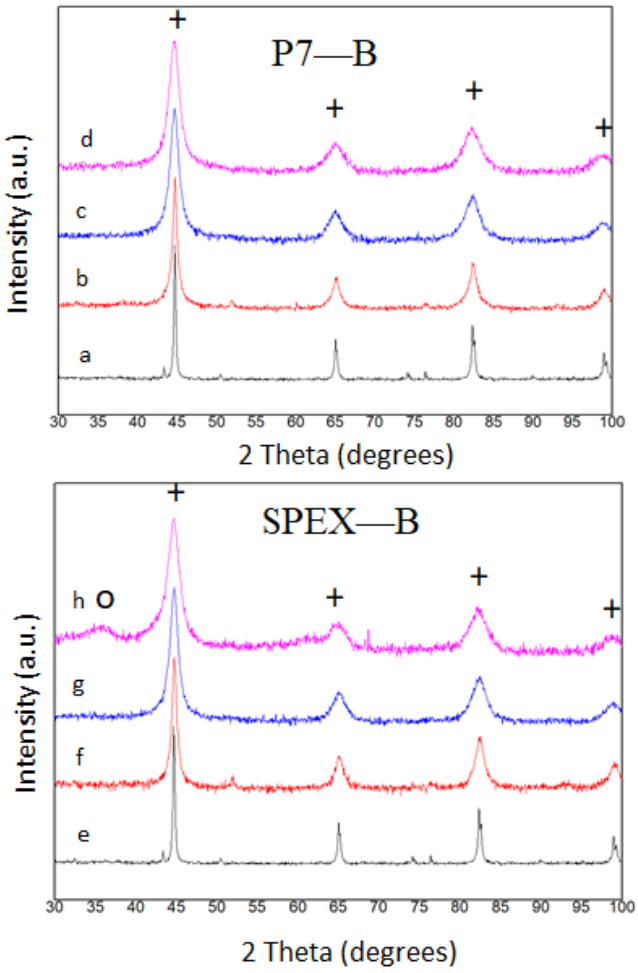

Figure 2. XRD diffraction patterns of alloy B ($Fe_{80}(NiZr)_7B_{12}Cu_1$). In the P7: (**a**) Before milling (0 h) and after milling ((**b**) 5 h, (**c**) 20 h, (**d**) 80 h); or in the Spex mill: (**e**) Before milling (0 h) and after milling ((**f**) 5 h, (**g**) 20 h, (**h**) 80 h). Bcc Fe rich solid solution (+), disordered phase (O).

If one focuses in the XRD patterns after 5 h of milling in alloy A (Figure 1a), the Nb peaks are still present. With the peak (110) of the Nb, it was verified that, at its lower angular reflection, we began to notice an asymmetry. The result of this asymmetry was clearer after 20 h of milling (in sample A), in which pattern appears a double peak in the place where before there was only one. Whereas in sample B, there only appears the new low angular phase. The proximity of the two peaks seems to indicate a mutual relationship. This new phase forcibly has a cell parameter slightly higher than that of the elemental Nb since it is shifted to lower angular positions. In short, asymmetry that began to be present at 5 h was an incipient peak of a new phase of Nb(B), which becomes more evident at 20 h. The creation of this phase is favored by the negative mixing enthalpy between Nb and B (−39 kJ/mol), indicating an exothermic process, which has also been detected in the scientific literature [13].

The formation of borides (undesired phases due to the associated loss of improved soft magnetic behavior) was not detected. After 80 h of milling (A alloy), in SPEX only the Fe rich bcc solid solution was detected, whereas a minor amount (2.1%) of the mechanically induced Nb(B) phase remains in alloy A milled in the P7 device.

The analysis of the XRD patterns of alloy B shows significative differences. The main phase is the bcc Fe rich phase and the reflections of minor phases disappears during milling. It should be remarked that the NiZr phase has not been detected after milling (probably the integration of Zr in the NiZr compound favors the integration of both elements in the main solid solution. From 80 h MA XRD diffraction patterns analysis, it was found that in

one case (milling in P7) there is only the majority solid solution; while in the other case (milling in SPEX), a highly disordered phase appears (about 3.2%). This phase has been previously detected [10] in alloys with Zr and is probably due to an incipient amorphous Zr rich phase.

The main parameters derived from the Rietveld refinement (Maud software); the lattice parameter, a, the crystalline size, L, and the microstrain, ε, were given in Tables 1–3, respectively (as a function of the milling time). The values are calculated with the isotropic model. Thus, they are calculated from refinement weighted analysis of the reflections of the bcc Fe rich phase, and the error is associated to both the isotropic model and the mixed refinement of all parameters.

Table 1. Lattice parameter, a (Å), of the cubic bcc Fe main phase.

Sample/Milling Time	0 h	5 h	20 h	80 h
P7—A	2.8608 ± 0.0001	2.8681 ± 0.0002	2.8731 ± 0.0002	2.8832 ± 0.0003
SPEX—A	2.8608 ± 0.0001	2.8659 ± 0.0001	2.8706 ± 0.0002	2.8694 ± 0.0002
P7—B	2.8608 ± 0.0001	2.8664 ± 0.0001	2.8699 ± 0.0002	2.8705 ± 0.0002
SPEX—B	2.8608 ± 0.0001	2.8642 ± 0.0002	2.8672 ± 0.0002	2.8719 ± 0.0003

Table 2. Crystalline size, L (nm), of the cubic bcc Fe main phase.

Sample/Milling Time	0 h	5 h	20 h	80 h
P7—A	237 ± 8	19.9 ± 0.9	14 ± 1	9.9 0.4
SPEX—A	237 ± 8	36 ± 3	15 ± 1	15 ± 1
P7—B	237 ± 8	29.3 ± 0.9	15.7 ± 0.6	13.4 ± 0.5
SPEX—B	237 ± 8	16.5 ± 0.9	11.5 ± 0.7	9.5 ± 0.5

Table 3. Microstrain, ε (%), of the cubic bcc Fe main phase.

Sample/Milling Time	0 h	5 h	20 h	80 h
P7—A	0.028 ± 0.003	0.10 ± 0.02	0.41 ± 0.08	0.66 ± 0.05
SPEX—A	0.028 ± 0.003	0.22 ± 0.02	0.42 ± 0.03	0.61 ± 0.02
P7—B	0.028 ± 0.003	0.02 ± 0.01	0.47 ± 0.02	0.59 ± 0.06
SPEX—B	0.028 ± 0.003	0.19 ± 0.02	0.44 ± 0.04	0.40 ± 0.03

The milling process favors the increase of the lattice parameter. This effect is due to the introduction of mechanically induced crystallographic defects (vacancies, dislocations) and to the solid solution of minor elements in the bcc phase. The highest value, 2.8832 ± 0.0003 Å, corresponds to alloy P7—A milled for 80 h. The lower values are found in samples without an additional second minor phase. Probably, these low parameters are due to the no solid solution of Nb and Zr (a high amount of Nb and Zr atoms remains in the Nb(B) and disordered phases, respectively).

The milling process favors the decrease of the crystalline size and the increase of the microstrain. It should be remarked that low crystalline size is calculated in those alloys (P7—A and SPEX—B milled for 80 h) with a minor secondary phase. One explication is that the Nb(B) and the disordered Zr rich phases formation favors the intra-division of the highly deformed crystals. The increase on the microstrain is due to the mechanically induced crystallographic defects.

The density of dislocation (of the bcc phase) was calculated (see Table 4) from crystallographic parameters (from Tables 2 and 3) by applying the following equation [14]:

$$\rho = 2 \times \sqrt{3}\,(\varepsilon / Lb), \quad (1)$$

Table 4. Dislocations density, ρ (10^{15} m^{-2}), of the cubic bcc Fe main phase.

Sample/Milling Time	0 h	5 h	20 h	80 h
P7—A	0.0323 ± 0.003	1.10 ± 0.09	4.58 ± 0.08	9.72 ± 0.07
SPEX—A	0.0323 ± 0.003	1.12 ± 0.08	4.44 ± 0.03	6.22 ± 0.05
P7—B	0.0323 ± 0.003	0.07 ± 0.05	4.91 ± 0.12	7.32 ± 0.08
SPEX—B	0.0323 ± 0.003	1.10 ± 0.09	4.11 ± 0.09	7.08 ± 0.07

In this equation, b is the Burgers vector. For the bcc crystallographic phase, the direction of easy dislocations concentration is (1 1 1). In this case, the Burgers vector is:

$$b = a\sqrt{3}/2, \quad (2)$$

The general trend, as expected, it is the increase of the dislocations density as increasing the milling time. Higher values are calculated in those samples milled (80 h) in the planetary mill. The results are close to the expected limit of the dislocation density (plastic deformation) in bcc Fe (10^{16} m^{-2}) [15]. It should be remarked than XRD methods sometimes can provide higher values of the dislocations density than transmission electron microscopy (TEM) analysis [16]. TEM values are considered as more accurate due to direct local observation. Nevertheless, the milling process favors inhomogeneity in the crystallographic defects.

The morphology of the powders after 80 h of milling was checked with SEM micrographs (as shown in Figure 3). There are rounded particles with smooth shape.

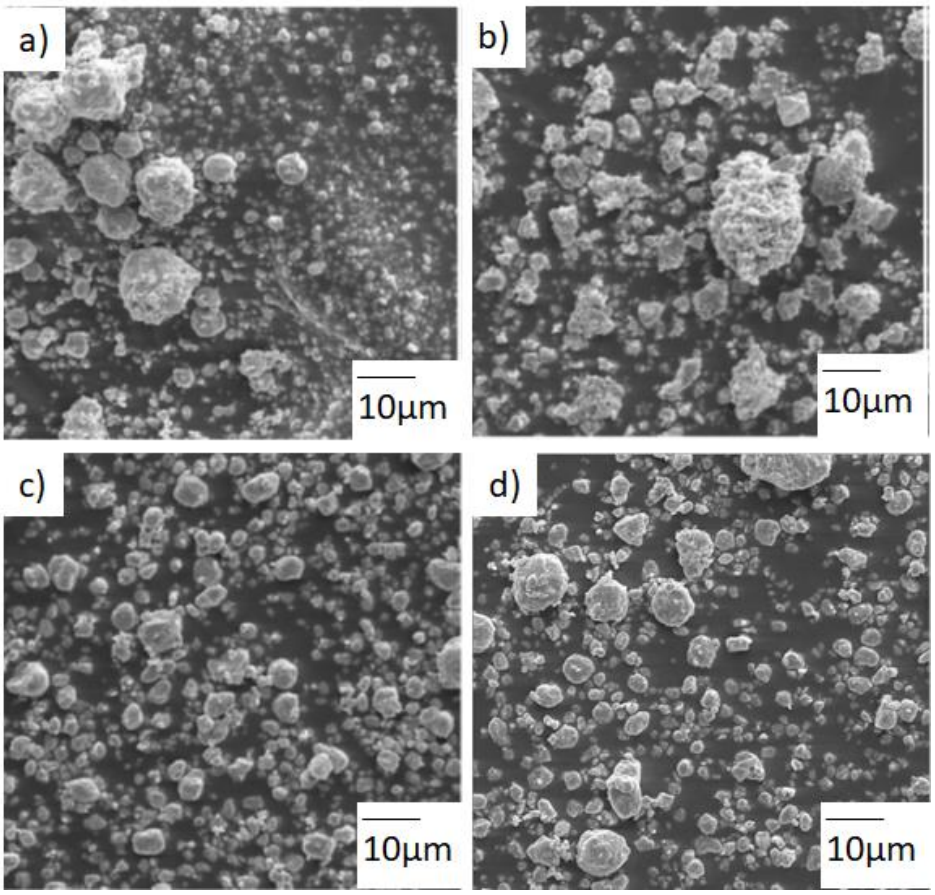

Figure 3. SEM micrographs after 80 h milling of samples: (**a**) P7—A, (**b**) SPEX—A, (**c**) P7—B, and (**d**) SPEX—B.

In order to analyze the particle size and its distribution, the particle size of several micrographs of each sample have been measured. The results are shown in Figure 4. To facilitate the comparison, the results were fitted with a log-normal distribution with the mean, μ, and the shape parameter (square root of variance), σ, values are given in Table 5.

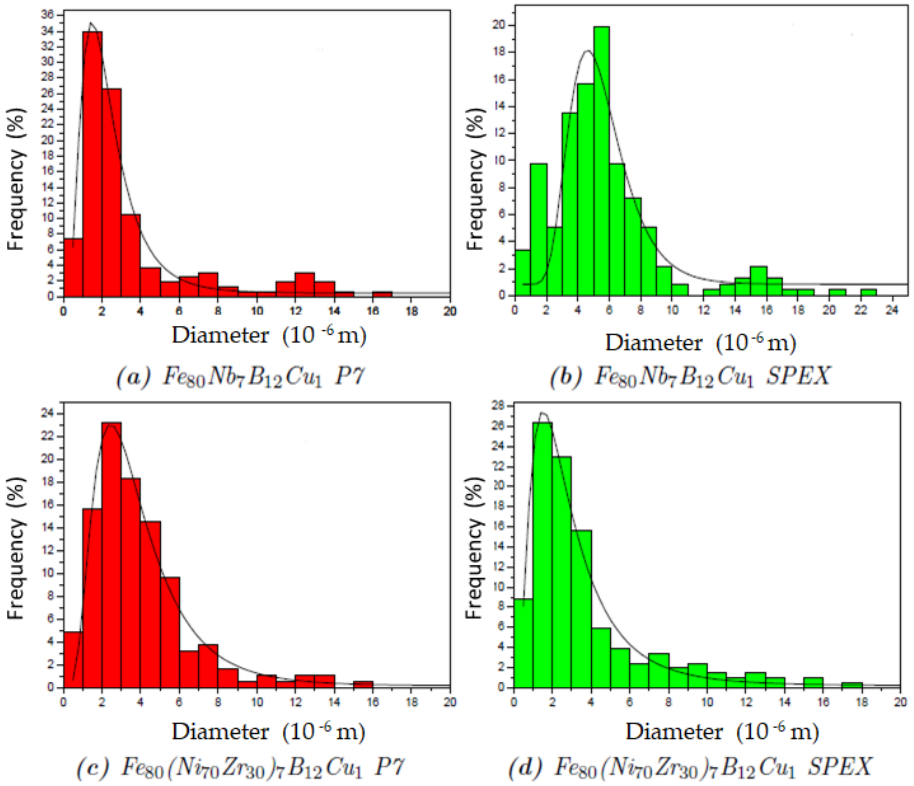

Figure 4. Particle size frequency distribution after 80 h milling of samples: (**a**) P7—A, (**b**) SPEX—A, (**c**) P7—B, and (**d**) SPEX—B.

Table 5. Parameters (mean, μ, and shape parameter, σ) of the log-normal distribution.

Sample	μ /10^{-6} m	σ /10^{-6} m
P7—A	2.4458	1.5367
SPEX—A	5.5279	1.9658
P7—B	3.9970	2.4863
SPEX—B	3.2053	2.5755

The higher mean value was found in sample SPEX—A, whereas the high shape parameter values are found in B samples. No correlation has been detected between these parameters (micrometric scale) and the XRD results (nanometric scale).

Likewise, compositional analysis was performed (80 h of milling) with EDS microanalysis. The measurements indicates that the contamination from the milling tools is lower than 1.5 ± 0.5 at.%; typical results coherent with those previously found [10,16]. Oxygen is also found, probably favored by the high surface area of the particles in contact with air after the milling process. Values are lower than 2.5 ± 0.5 at.%.

Additional thermal analysis has been performed from DSC scans. The analysis of the evolution of the thermal behavior has been carried out after 5, 20, and 80 h of milling at 10 K/min as the heating rate. The DSC scans (5 to 80 h of milling) of A and B samples are given in Figures 5 and 6, respectively. DSC after 80 h of milling were reported on ref. [17]. Here we discuss the process evolution and the kinetic analysis.

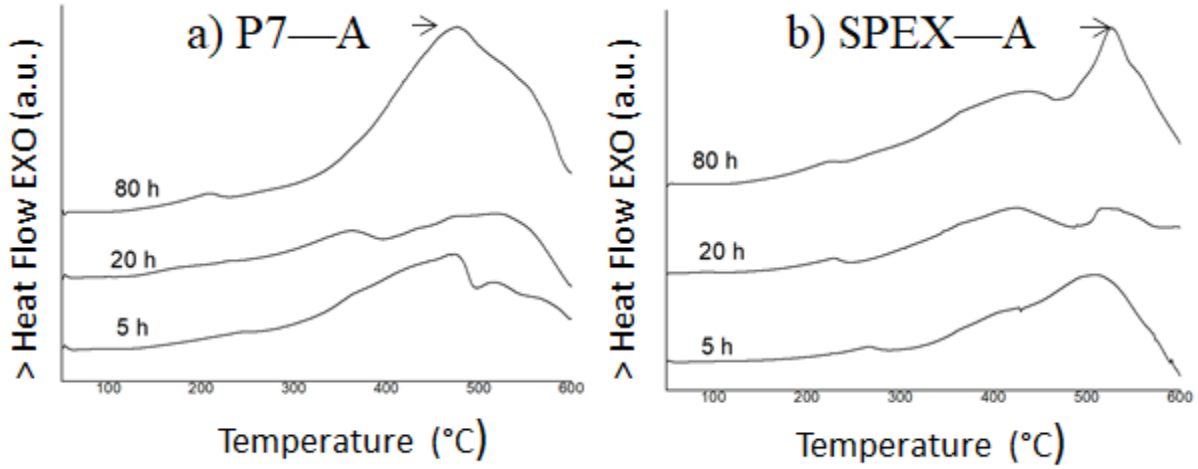

Figure 5. DSC (differential scanning calorimetry) scans of alloy A after milling (5, 20, 80 h) in the P7 (**a**) or in the Spex (**b**) mill.

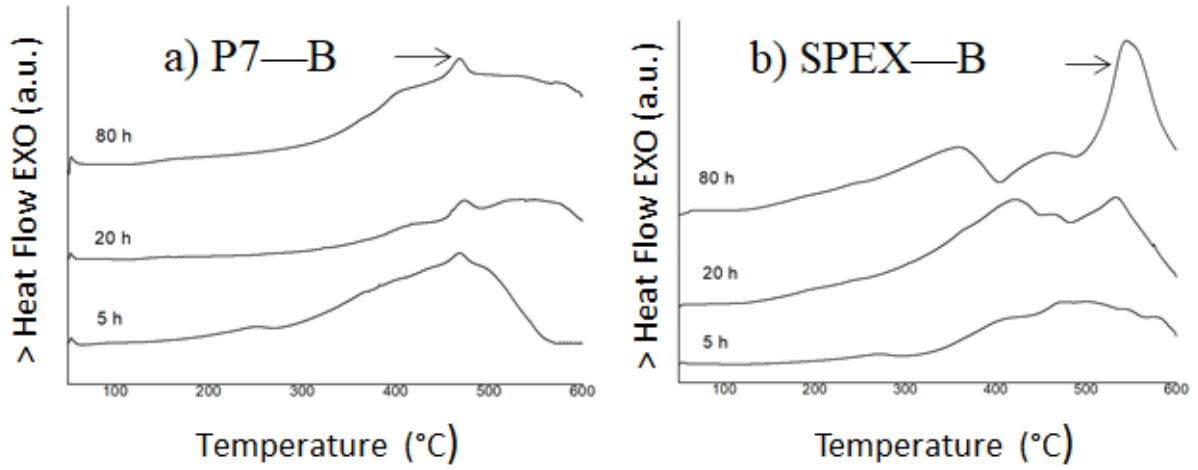

Figure 6. DSC scans of alloy B after milling (5, 20, 80 h) in the P7 (**a**) or in the Spex (**b**) mill.

In all scans, multiple exothermic processes are observed in wide intervals of temperature and with a certain degree of overlap. Exothermic processes at lowest temperature (below 400 °C) were associated with relaxation phenomena (caused by a decrease of the free volume after relaxation of the mechanically induced tensions at the micro and nanoscale). Furthermore, thermal treatment also favors the reduction of the crystallographic defects and local inhomogeneity by atomic diffusion. The exothermic processes at higher temperatures were associated with crystallization (nucleation and/or crystalline growth). This complex behavior is typical of nanocrystalline alloys produced by mechanical alloying [9,18]. In all DSC at 80 h, the main peak is remarked with an arrow. The peak temperature is higher (T_p > 500 °C) in samples milled with a shaker mill if compared with the temperature of the samples milled in the planetary mill (T_p < 500 °C). Probably, higher energetic milling favors higher internal local temperature and atomic diffusion [18].

On the other hand, the apparent activation of the crystallization processes (those remarked with an arrow) has also been calculated by applying Kissinger's linear method at heating rates of 10, 20, 30, and 40 K/min. Kissinger's method is based on the relationship between the peak temperature, T_p, and the scan rate, β. The linear fitting is shown in Figure 7, and the apparent activation energies are given in Table 6. The activation energy is determined from the slope of the linear fit, by applying the following relation (R is the universal gas constant):

$$E = -R/(1000\ T_p), \quad (3)$$

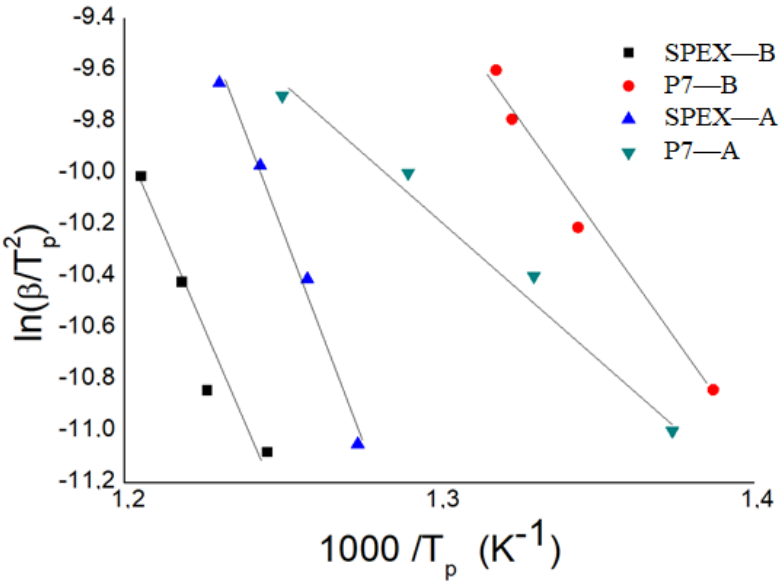

Figure 7. Kissinger linear fitting to calculate the activation energy of the crystallization process (experimental point for each sample are linked to peak temperatures of samples determined at 10, 20, 30, and 40 K/min from right to left respectively). Coefficients of correlation R-squared > 0.9.

Table 6. Apparent activation energy of the crystallization process.

Sample	E kJ mol^{-1}
P7—A	87 ± 11
SPEX—A	263 ± 21
P7—B	144 ± 13
SPEX—B	225 ± 44

The activation energies are higher in samples milled in the shaker mill, and a possible hypothesis is that it was favored by different milling energy transfer (higher energy can favor diffusion and the homogeneity of the alloys, stabilizing against crystalline growth). Local inhomogeneities can act as preferential sites for crystalline growth, reducing the activation energy. An alternative hypothesis is the content of oxygen, higher (~0.5–0.8 at.%) in powders milled in the shaker mill. More work will be provided to reach a definitive explanation. Likewise, the energy of activation values were characteristic for each type of reaction [19]. According to the bibliography, the activation energy for the crystal growth of Fe based nanocrystalline samples are around 140 kJ/mol [20] for pure iron. In samples containing additional elements, these energies can have higher/lower values. In Fe-Co-Nb-B alloys obtained by MA, energies between 238 and 261 kJ/mol have been calculated [21]. For amorphous samples in which a new phase must be nucleated, energies have values and are around 300 kJ/mol [22] or 365 kJ/mol [23], or even 425 and 550 kJ/mol in Fe-Nb-B alloys [24].

Thus, all of the analyzed crystallization process can be associated to the crystalline growth of the pre-existing Fe rich solid solution.

3.2. Mills Comparison

If we compare the phases detected by XRD after 80 h of milling, it is found that:

(a) In the composition with Nb milled in SPEX, only the Fe rich solid solution has been detected. Whereas, in the Nb alloy milled in P7, the major phase is the Fe rich bcc phase coexisting with a low amount of a Nb(B) phase.

(b) In the composition with Zr milled in SPEX, the Fe rich solid solution coexists with a minor disordered phase. Whereas, in the alloy milled in P7, this phase was not formed.

The results indicate that probably the milling is more energetic and efficient in SPEX. In one case, at 80 h in the P7, it was not possible to obtain a single phase (it would surely be necessary to increase the milling time to promote the Nb(B) phase disappearance and the integration of the Nb, via solid solution or in the grain boundaries). In the other, in the SPEX, the more energetic milling favors the formation of a disordered phase.

Likewise, from DSC scans we can state that the higher thermal stability (of the analyzed crystallization process) was found in the samples milled in the shaker mill. The criteria for a higher thermal stability of the nanocrystalline phase were high temperature of transformation and high activation energy.

A comparative study was performed to analyze the transfer of energy in both milling devices. This factor must influence the milling time needed to develop specific microstructural changes, such as nanocrystallinity. In the bibliography, there are multiple comparative studies between ball milling devices at the laboratory level. These are based on the comparison via experimental data and/or simulations. Overall, these studies usually conclude that the planetary mills were less energetic than the shaker mills as SPEX. Mathematic ab initio models have been applied to study MA process [25]. Moreover, experimental data to determine the speed of balls or rotation of milling vials [26]. These works are generally based on energy transferred during milling [27]. To make a comparison a useful parameter was the ratio between the power transmitted and the powder mass (P/m).

One of the problems associated with the energetic comparison of mills is the differences in the motion. Another question is that the factors involved are multiple and there are complex relationships between them: Rotation frequencies, number and characteristics of the balls, geometry vials, degree of container filling, powder mass, energy transfer, temperature, milling atmosphere, frequency of interactions, etc. Furthermore, real processes have a distribution of energies involved in collisions due to a distribution of ball velocities in the shocks [28]. Some of the studies carried out take into account the direct comparison of shaker Spex and planetary mills [19,29].

First, for the comparison between both devices, we apply the method described in ref. [29]. In order to evaluate the total energy transferred to the powder during milling, it is necessary to know the ball velocity. In the Spex device, the ball velocity given in ref. [29] is v = 2.5 m/s. To have an equivalent value in the P7, the following formula has been chosen to determine the speed, v, of ball impact [30].

$$v^2 = (r_p\,\Omega)^2 + (r_j - r_b)^2\,\omega^2\,(1 + (2\omega/\Omega) \quad (4)$$

As introduced in the Section 2, in SPEX the cycles are 875 rpm, whereas in the P7 the selected number of cycles (jar, platform) is $\omega = \Omega = 600$ rpm. The P7 radius of the platform $r_p = 7$ cm, the ball radius r_b is 0.5 cm for P7; and the internal radius of the jar $r_j = 1.7$ cm. The calculated velocity is v = 0.79 m/s. Obviously, these values should be considered for devices comparison, and real energy transfers have a distribution of speeds. Other models provide different velocities, as an example, the expression of reference [31] provides a value of v = 2.04 m/s for P7.

Regarding the kinetic energy, E_c, transferred by a ball in the planetary mill, it can be calculated directly from the velocity. The calculated value is 0.002 J. The equivalent calculation in the shaker was calculated in ref. [29], and the kinetic energy is 0.026 J.

The normalized (by unit mass of powder) total energy (E/m) transferred at a given milling time, t, was calculated by taking into account the following expression [32]:

$$E/m = (nE_c t/m) \quad (5)$$

where n is the balls number. As shown in Table 7, the calculated values for 80 h of milling are $(E/m)_{SPEX} = 5193$ J/g and $(E/m)_{P7} = 3752$ J/g. Thus, milling is more energetic in the Spex device.

Table 7. Ball velocity, kinetic energy, and total energy of Spex and P7.

Mill	Ball Velocity m/s	Kinetic Energy J	(E/m) J/g
P7	0.79	0.002	3752
SPEX	2.5	0.026	5193

The applied model considers that the frequency of impacts (events frequency) is equivalent in both devices. This factor is inversely proportional to the time between shock events on milling. The sliding factor influences the time it takes for the balls to separate from the container wall, the takeoff time, t_t. The increase in this time reduces the frequency of collisions. It is also necessary to determine a flight time of the ball before impact. Obviously, there is a distribution of speeds as well as energy and time. However, it should be taken into account that we need to stablish an easy way to compare both devices with characteristic mean parameters.

The ball detaches from the container wall when the value of the contact force is zero. The takeoff time can be estimated by applying the following expression [33]:

$$t_t = (1/(\Omega + \omega)) \arccos(-(\omega^2 r/\Omega^2 R)), \quad (6)$$

In the P7 device this time is $t_t = 0.076$ s. Likewise, the flight time t_f (between detachment and collision) is also linked to the period (inverse of the frequency) in planetary mills. Thus, the period is higher in P7. The P7 flight time is determined by using the relationship given in Figure 8 [19]. The calculated time is $t_f = 0.013$ s.

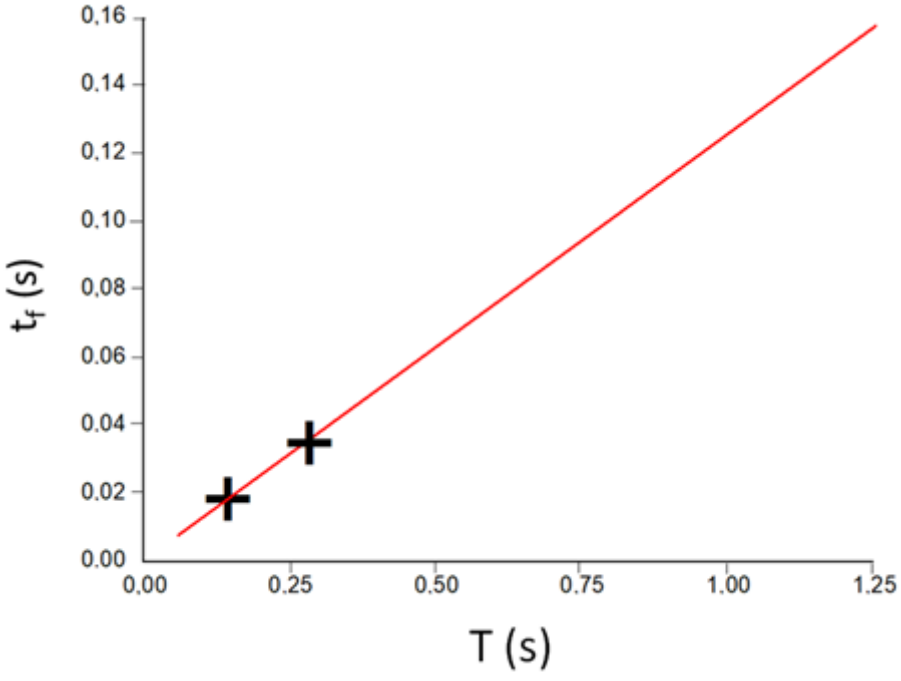

Figure 8. Flight time, t_f, as a function of the period T, (+, this work; red line, [19]).

Consequently, the total time [19], its sum, is $t_t + t_f$ (P7) = 0.089 s. In the SPEX device, the bibliography data were used: $t_t = 0.0073$ s and $t_f = 0.0269$ s that drive to $t_t + t_f$ (SPEX) = 0.0342 s. As the total time is higher in the planetary mill, the events frequency (for unit time) is higher in the shaker mill.

Thus, from the time between collisions, the shaker mill is also more effective. Likewise, the results obtained in this study cannot be directly based in this total time because the final microstructure varies (sometimes appears a second minor phase).

Therefore, SPEX mill is more energetically efficient than the P7 planetary mill (in the processing conditions of our study).

On the other hand, it is possible to calculate an equivalent milling time between different mills [34,35]. The calculation of this equivalent time is based on the assumption that the power transferred per unit of mass (P/m) is directly proportional to the time so that in two different devices the powder achieves the same final microstructure. It can be determined by applying the following equation:

$$(P/m)_{SPEX} = \varphi\ (P(\Omega_o)/m)_{P7}\ (\Omega/\Omega_o)^3, \quad (7)$$

This approach has been previously applied in FeNb and FeZr alloys [35]. In our study, the cycles ratio in the P7 is 1 ($\Omega = \Omega_o = 600$ rpm). From the previous calculations, we can calculate φ that is a proportionality factor, $\varphi = 1.384$. Thus, equation 6 is reduced to:

$$(P/m)_{SPEX} = \varphi\ (P(\Omega_o)/m)_{P7}, \quad (8)$$

The equivalent milling time, t_{eq}, can be calculated by applying [19]:

$$t_{eq} = ((P/m)_{SPEX}/(P(\Omega_o)/m)_{P7})\ t, \quad (9)$$

It has been estimated (from Table 7 data) that the time required in the P7 for the same energy transfer is 1.384 higher than for SPEX. Obviously, there are many factors modifying the consequences of this equivalent time. Sometimes the MA process is not energetic enough to obtain a concrete microstructure. For example, by modifying the milling conditions, the achieved microstructure can be nanocrystalline or amorphous [36]. Other possibilities are that the energy transfer facilitates the extension of the solubility limits or the formation of intermetallic compounds [24,37]. In alloy A, the energy/power transfer is not enough to obtain only the bcc Fe rich solid solution in the planetary mill (Nb(B) phase remains after 80 h of milling), and in alloy B the high energy/power transfer in shaker mill favors the formation of an incipient amorphous phase. Additional experiments, with alloys of similar composition and/or by repeating production process will confirm the general trend found in this work.

4. Conclusions

Two alloys, $Fe_{80}Nb_7B_{12}Cu_1$ (A) and $Fe_{80}(NiZr)_7B_{12}Cu_1$ (B), have been produced in two milling devices, a shaker mill (SPEX) and a planetary mill (P7). In the sample A milled in the shaker device and in sample B milled in the planetary mill only an Fe rich solid solution was detected by XRD after 80 h of MA. Instead, in the sample A milled in the planetary mill a low percentage of a Nb(B) phase was also detected; whereas in the sample B shaker milled the Fe rich solid solution coexist with a minor disordered phase. Additional thermal analysis permits us to establish that the analyzed crystallization process is due to crystalline growth, and the thermal stability is higher in samples milled in the shaker mill (higher temperature of crystallization and activation energy).

The results indicate that probably the milling is more energetic and efficient in the shaker mill. The equivalent time required in the planetary mill for the same energy transfer is 1.384 higher. In alloy A, the energy/power transfer is not enough to obtain only the bcc Fe rich solid solution in the planetary mill (a minor Nb(B) phase remains), and in sample B the high energy/power transfer in shaker mill favors the formation of a disordered Zr rich phase.

Author Contributions: Methodology, L.E., J.S.; formal analysis, A.C.; investigation, A.C.; writing—original draft preparation, J.-J.S. All authors have read and agreed to the published version of the manuscript.

Funding: This research was funded by Spanish MINECO project MAT2016-75967-P and UdG project PONTOS-2020/01.

Institutional Review Board Statement: Not applicable.

Informed Consent Statement: Not applicable.

Data Availability Statement: The data presented in this study are available on request from the corresponding author.

Acknowledgments: The authors agree the Technical Research Facilities of the University of Girona.

Conflicts of Interest: The authors declare no conflict of interest.

References

1. Kwon, S.; Kim, S.; Yim, H.; Kang, K.H.; Yoon, C.S. High saturation magnetic flux density of novel nanocrystalline core annealed under magnetic field. *J. Alloys Comp.* **2020**, *826*, 154136. [CrossRef]
2. Alleg, S.; Ibrir, M.; Fenineche, N.E.; Azzaza, S.; Bensalem, R.; Suñol, J.J. Magnetic and structural characterization of the mechanically alloyed $Fe_{75}Si_{15}B_{10}$ powders. *J. Alloys Comp.* **2010**, *494*, 109–115. [CrossRef]
3. Parsons, R.; Zang, B.; Onodera, K.; Kishimoto, H.; Kato, A.; Suzuki, K. Soft magnetic properties of rapidly-annealed nanocrystalline Fe-Nb-B-(Cu) alloys. *J. Alloys Comp.* **2017**, *723*, 408–417. [CrossRef]
4. Suryanarayana, C. Mechanical alloying and milling. *Prog. Mater. Sci.* **2001**, *46*, 1–184. [CrossRef]
5. Suzuki, K.; Kataoka, N.; Inoue, A.; Makino, A.; Masumoto, T. High saturation magnetization and soft magnetic properties of bcc Fe-Zr-B alloys with ultrafine grain structures. *Mater. Trans.* **1990**, *31*, 743–746. [CrossRef]
6. Fan, X.; Tang, Y.; Shi, Z.; Jiang, M.; Shen, B. The effect of Ni addition on microstructure and soft magnetic properties of FeCoZrBCu nanocrystalline alloys. *AIP Adv.* **2017**, *7*, 056107. [CrossRef]
7. Alleg, S.; Chabi, T.; Bensebaa, N.; Saurina, J.; Escoda, L.; Hlil, E.K.; Suñol, J.J. Investigation on the critical behavior, magnetocaloric effect and hyperfine structure in the $Fe_{72}Nb_8B_{20}$ powders. *Materials* **2020**, *13*, 4476. [CrossRef] [PubMed]
8. Ipus, J.J.; Blázquez, J.S.; Franco, V.; Lozano-Pérez, S.; Conde, A. Role of the starting phase of boron on the mechanical alloying of FeNbB composition. *J. Alloys Comp.* **2013**, *553*, 119–124. [CrossRef]
9. Chabi, T.; Bensebaa, N.; Alleg, S.; Azzaza, S.; Suñol, J.J.; Hlil, E.K. Effect of the boron content on the amorphization process and magnetic properties of the mechanically alloyed $Fe_{92-x}Nb_8B_x$ powders. *J. Supercond. Novel Magn.* **2019**, *32*, 893–901. [CrossRef]
10. Pilar, M.; Suñol, J.J.; Bonastre, J.; Escoda, L. Influence of process control agents in the development of a metastable Fe-Zr based alloy. *J. Non-Cryst. Solids* **2007**, *353*, 848–850. [CrossRef]
11. Djilali, Z.; Said, B. Study of the ball milling device for synthesizing nanocrystalline powder. *J. Nano Res.* **2017**, *47*, 60–70. [CrossRef]
12. Lutterotti, L.; Matthies, S.; Wenk, H.R. Quantitative phase analysis. *Newsl. CPD* **1999**, *21*, 14–15. [CrossRef]
13. Alleg, S.; Kartout, S.; Ibrir, M.; Azzaza, S.; Fenineche, N.E.; Suñol, J.J. Magnetic, structural and therml properties of the Finemet-type powders prepared by mechanical alloying. *J. Phys. Chem. Solids* **2013**, *74*, 550–557. [CrossRef]
14. Eckert, J.; Holzer, J.C.; Krill, C.E.; Johnson, W.L. Structural and thermodynamic properties of nanocrystalline fcc metals prepared by mechanical attrition. *J. Mater. Res.* **1992**, *7*, 1751–1761. [CrossRef]
15. Ibn Gharsallah, H.; Azabou, M.; Escoda, L.; Suñol, J.J.; López, I.; Llorca-Isern, N. The magnetic and structural properties of $(Fe_{75}Al_{25})_{100-x}B_x$alloys prepared by mechanical alloying. *J. Alloys Comp.* **2017**, *729*, 776–786. [CrossRef]
16. Takebayashi, T.; Kunieda, T.; Yoshinaga, N.; Ushioda, K.; Ogata, S. Comparison of the dislocation density in martensitic steels evaluated by some X-ray diffraction methods. *ISIJ Inter.* **2010**, *50*, 875–882. [CrossRef]
17. Carrillo, A.; Escoda, L.; Saurina, J.; Suñol, J.J. Structural and magnetic behavior of Fe(Nb,Zr) rich alloys produced by mechanical alloying. *AIP Adv.* **2018**, *8*, 047704. [CrossRef]
18. Abdoli, H.; Ghanbari, H.; Baghshahi, S. Thermal stability of nanostructured aluminium powder synthesized by high energy milling. *Mater. Sci. Eng. A* **2011**, *528*, 6702–6707. [CrossRef]
19. Ipus, J.J. Microstructure and Thermomagnetic Behavior of (FeCo)(NbZr)(GeB) Alloys Prepared by Milling. Ph.D. Thesis, Universidad de Sevilla, Sevilla, Spain, 2009.
20. Ye, F.; Lu, K. Crystallization kinetics of Al-La-Ni amorphous alloy. *J. Non-Cryst. Solids* **2000**, *262*, 228–235. [CrossRef]
21. Liu, Y.; Chang, I.; Lees, M. Thermodynamic and magnetic properties of multicomponent $(Fe,Ni)_{70}Zr_{10}B_{20}$ amorphous alloy powders made by mechanical alloying. *J. Mater. Sci. Eng.* **2001**, *304–306*, 992–996. [CrossRef]
22. Suñol, J.J.; Güell, J.M.; Bonastre, J.; Alleg, S. Structural study of nanocrystalline Fe-Co-Nb-B alloys prepared by mechanical alloying. *J. Alloys Comp.* **2009**, *483*, 604–607. [CrossRef]
23. Krakhmalev, P.V.; Yi, D.; Nyborg, L.; Yao, Y. Isothermal grain growth in mechanically alloyed nanostructured $Fe_{80}Ti_8B_{12}$alloy. *Mat. Lett.* **2003**, *57*, 3671–3675. [CrossRef]
24. Johnson, F.; Hughes, P.; Gallagher, R.; Harris, V. structure and magnetic properties of new FeCo-based nanocrystalline ferromagnets. *IEEE Trans. Magn.* **2001**, *37*, 2261–2263. [CrossRef]
25. Ipus, J.J.; Blázquez, J.S.; Conde, C.F.; Borrego, J.M.; Franco, V.; Lozano-Pérez, S.; Conde, A. Relationship between mechanical amorphization and boron integration during processing of FeNbB alloys. *Intermetallics* **2014**, *49*, 98–105. [CrossRef]
26. Chattopadhyay, P.; Manna, I.; Talapatra, S.; Pabi, S. A mathematical analysis of milling mechanics in a planetary ball mill. *Mater. Chem. Phys.* **2001**, *68*, 85–94. [CrossRef]

27. Basset, D.; Matteazi, P.; Miani, F. Measuring the impact velocities of balls in high energy mills. *Mater. Sci. Eng. A* **1994**, *174*, 71–74. [CrossRef]
28. Concas, A.; Pisu, M.; Lai, N.; Cao, G. Modelling of comminution in processes in Spex Mixer/Mill. *Chem. Eng. Sci.* **2006**, *61*, 3746–3760. [CrossRef]
29. Dastanpoor, E.; Enayati, M.H. Effect of milling intensity on mechanical alloying of Cu-Zr-Al system. *Ind. J. Eng. Mater. Sci.* **2015**, *22*, 521–526.
30. Gheisari, K.; Oh, J.T.; Javadpour, S.; Ghaffari, M.J. The effect of milling speed on the structural properties of mechanically alloyed Fe-45% Ni powders. *J. Alloys Comp.* **2009**, *472*, 416–420. [CrossRef]
31. Magini, M. The role of energy transfer in mechanical alloying powder processing. *Mater. Sci. Forum* **2009**, *88*, 121–128. [CrossRef]
32. Singh, S.; Godkhindi, M.M.; Krishmarao, R.V.; Murty, B.S. Effect of milling energy on mechanical activation of (Mo+Si_3N_4) powders during the synthesis of Si_3N_4-$MoSi_2$in situ composites. *J. Euro. Ceram. Soc.* **2009**, *29*, 2069–2077. [CrossRef]
33. Karthik, B.; Sai Gautam, G.; Karthikeyan, N.R.; Murty, B.S. Analysis of mechanical milling in Sismoloyer: An energy modeling approach. *Metall. Mater. Trans. A Phys. Metall. Mater. Sci.* **2012**, *43*, 1323–1327. [CrossRef]
34. Ipus, J.J.; Blázquez, J.S.; Franco, V.; Millán, M.; Conde, A.; Oleszak, D.; Kulik, T. An equivalent time approach for scaling the mechanical alloying process. *Intermetallics* **2008**, *16*, 470–478. [CrossRef]
35. Blázquez, J.S.; Ipus, J.J.; Conde, C.F.; Conde, A. Comparison of equivalent ball milling process on $Fe_{70}Zr_{30}$ and $Fe_{70}Nb_{30}$. *J. Alloys Comp.* **2012**, *536*, 9–12. [CrossRef]
36. Martin, G.; Gaffet, E. Mechanical alloying: Far from equilibrium phase transitions. *Colloq. Phys.* **1990**, *51*, 71–77. [CrossRef]
37. Nova, K.; Novak, P.; Prusa, F.; Kopecek, J.; Cech, J. Synthesis of intermetallics in Fe-Al-Si system by mechanical alloying. *Metals* **2019**, *9*, 20. [CrossRef]